RMD-1, a novel microtubule-associated protein, functions in chromosome segregation in *Caenorhabditis elegans*

Kumiko Oishi,[1] Hideyuki Okano,[2] and Hitoshi Sawa[1,3]

[1]Laboratory for Cell Fate Decision, RIKEN Center for Developmental Biology, Chuo-ku, Kobe 650-0047, Japan
[2]Department of Physiology, Keio University School of Medicine, Shinjuku-ku, Tokyo 160-8582, Japan
[3]Department of Biology, Graduate School of Science, Kobe University, Nada-ku, Kobe 657-8501, Japan

For proper chromosome segregation, the sister kinetochores must attach to microtubules extending from the opposite spindle poles. Any errors in microtubule attachment can induce aneuploidy. In this study, we identify a novel conserved *Caenorhabditis elegans* microtubule-associated protein, regulator of microtubule dynamics 1 (RMD-1), that localizes to spindle microtubules and spindle poles. Depletion of RMD-1 induces severe defects in chromosome segregation, probably through merotelic attachments between microtubules and chromosomes. Although *rmd-1* embryos also have a mild defect in microtubule growth, we find that mutants of the microtubule growth regulator XMAP215/ZYG-9 show much weaker segregation defects. This suggests that the microtubule growth defect in *rmd-1* embryos does not cause abnormal chromosome segregation. We also see that RMD-1 interacts with aurora B in vitro. Our results suggest that RMD-1 functions in chromosome segregation in *C. elegans* embryos, possibly through the aurora B–mediated pathway. Human homologues of RMD-1 could also bind microtubules, which would suggest a function for these proteins in chromosome segregation during mitosis in other organisms as well.

Introduction

Proper chromosome segregation is required to maintain genetic materials and prevent aneuploidy, which leads to genetic diseases and cancers (Cimini and Degrassi, 2005). Chromosome segregation is exerted by a bipolar spindle that is created by the attachment of each sister chromatid to microtubules (i.e., kinetochore microtubules) derived from the opposite spindle poles. After the nuclear envelope breaks down, the microtubules probe 3D space and eventually encounter their target, a kinetochore. Initially, one of the sister kinetochores is captured by the lateral surface of a microtubule, causing the chromatid to move rapidly toward the microtubule's pole of origin. Once end-on attachment of the microtubule to the kinetochore occurs, microtubules emanating from the opposite spindle pole soon achieve interactions with the remaining unattached sister kinetochore, resulting in correct attachment between the spindle and the chromosome (amphitelic attachment; Pinsky and Biggins, 2005). Thereafter, the microtubules at the opposite poles gradually move the chromosome into position at the mitotic plate.

The correct attachment of kinetochore microtubules to chromatids is achieved by stochastic events termed search and capture, which are based on the dynamic instability of microtubule plus ends, which switch between growing and shrinking phases (Mitchison and Kirschner, 1984). Therefore, attachment errors such as monotelic, syntelic, and merotelic attachment occur frequently, even in normal cells, but are corrected until anaphase onset (Pinsky and Biggins, 2005). Monotelic attachments, in which only one of the sister kinetochores is attached to spindle microtubules, are frequent in the early stages of mitosis. Syntelic attachments are those in which both sister kinetochores are attached to microtubules from the same spindle pole. Finally, merotelic attachments occur when a single kinetochore becomes attached to microtubules from both spindle poles rather than just one.

The spindle checkpoint, a cell cycle protection mechanism, prevents the metaphase to anaphase transition until all of the chromosomes attach properly with microtubules (Lew and Burke, 2003).

Correspondence to Hitoshi Sawa: sawa@cdb.riken.jp

Abbreviations used in this paper: hRMD, human RMD; MAP, microtubule-associated protein; MCAK, mitotic centromere-associated kinesin; NEBD, nuclear envelope breakdown; Psa, phasmid socket absent; rDNA, ribosomal DNA; RMD, regulator of microtubule dynamics; SNP, single-nucleotide polymorphism.

The online version of this article contains supplemental material.

The Journal of Cell Biology, Vol. 179, No. 6, December 17, 2007 1149–1162
http://www.jcb.org/cgi/doi/10.1083/jcb.200705108

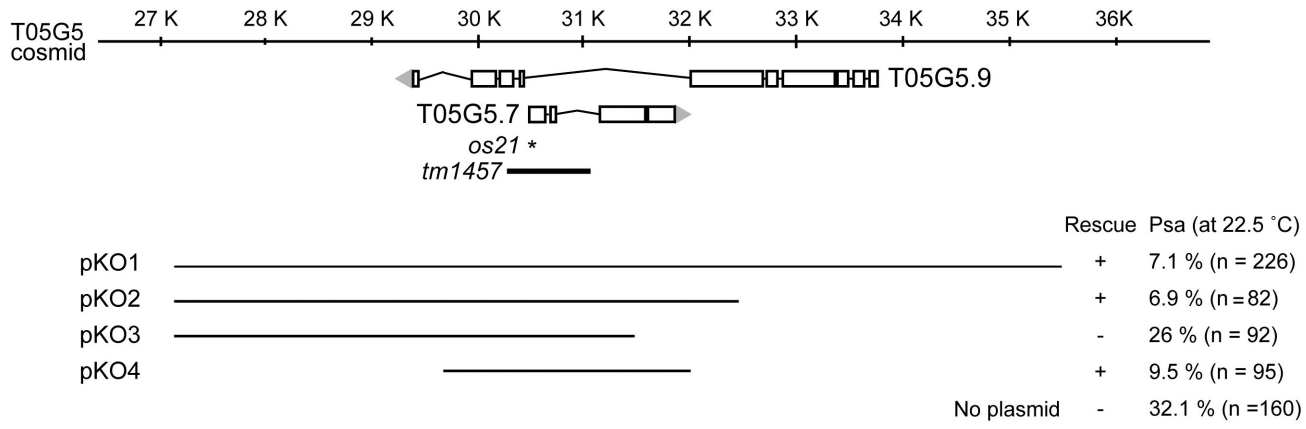

Figure 1. **Positional cloning of *rmd-1*.** Plasmids containing the indicated genomic fragments were tested for rescue of the Psa phenotype of *rmd-1(os21)*. The results are shown at the right. The numbers at the top indicate positions in the T05G5 cosmid. The asterisk represents the position of a mutation in *os21* mutants.

The spindle checkpoint is thought to sense kinetochore attachments and tension at kinetochores generated by kinetochore microtubules (Pinsky and Biggins, 2005). In monotelic attachments, unattached kinetochores are sensed by the spindle checkpoint and generate a signal to delay anaphase onset until the remaining unattached sister kinetochore is properly attached (Musacchio and Hardwick, 2002). In syntelic attachments, weak or absent tension at the kinetochores is thought to activate the spindle checkpoint, leading to the destabilization of microtubule attachments through aurora B kinase (Tanaka et al., 2002). In contrast, merotelic attachments put enough tension on kinetochores without activating the spindle checkpoint. Nonetheless, merotelic attachments must usually be corrected before anaphase because they are frequently observed in the early prometaphase of normal cells, but the resultant lagging chromosomes are rarely seen in cells entering anaphase (Cimini et al., 2003). Recent studies have shown that depletion of a microtubule destabilization factor, KinI/mitotic centromere-associated kinesin [MCAK]/XKCM1, from the centromere induces merotelic attachments (Kline-Smith et al., 2004). It has been proposed that phosphorylation of MCAK by aurora B kinase is involved in the correction mechanisms of incorrect attachments (Ohi et al., 2003). However, it is not clear how MCAK–aurora B recognizes incorrect attachments.

In addition to the microtubule destabilization factor, some microtubule-associated proteins (MAPs) that promote the outgrowth of kinetochore microtubules localize to the kinetochore. A *Drosophila melanogaster* CLASP (cytoplasmic linker protein–associated protein) homologue, Orbit/Mast, is required for chromosome alignment, kinetochore–microtubule attachment, and maintenance of spindle bipolarity (Inoue et al., 2000; Lemos et al., 2000; Maiato et al., 2002). In budding and fission yeast, another set of MAPs, the XMAP215 homologues, are present at the kinetochore and contribute to chromosome segregation (Ohkura et al., 2001). In *Caenorhabditis elegans*, a CLASP homologue, CLS-2, localizes to the kinetochores and is required for chromosome alignment (Cheeseman et al., 2005). An XMAP215 homologue, ZYG-9, regulates the growth of astral microtubules (Matthews et al., 1998); however, the role of ZYG-9 in chromosome segregation has not been investigated.

We identified a *C. elegans* gene, regulator of microtubule dynamics 1 (*rmd-1*), which is a member of a novel conserved MAP family. Depletion of RMD-1 caused strong defects in chromosome segregation, which were probably caused by merotelic attachments. RMD-1 interacted with AIR-2/aurora B kinase in vitro, suggesting that RMD-1 functions with AIR-2 in chromosome segregation. In addition to the defects in chromosome segregation, *rmd-1(RNAi)* embryos showed weak but significant defects in microtubule outgrowth. However, the loss of ZYG-9/XMAP215, a main regulator of microtubule outgrowth, caused much less severe defects in chromosome segregation than that of RMD-1. These results suggest that in addition to regulating microtubule outgrowth, RMD-1 has specific functions in the execution of proper chromosome segregation, probably by preventing abnormal attachments.

Results

rmd-1 encodes a novel protein with multiple coiled-coil domains that is conserved in human, mouse, *Xenopus laevis*, and zebrafish

rmd-1(os21) was identified in a screen for mutants that lacked phasmid socket cells in the tail (phasmid socket absent [Psa] phenotype; Sawa et al., 2000). *rmd-1(os21)* animals showed the Egl (egg laying defective) and Psa (25% [$n = 44$] or 33.2% [$n = 334$] with or without maternal contributions, respectively) phenotypes at 25°C. In addition, *rmd-1(os21)* displayed temperature-sensitive maternal effect lethality (100% [$n = 138$]) at 25°C.

The *rmd-1* gene was mapped to a region between *ced-7* and *unc-69* on chromosome III. Single-nucleotide polymorphisms (SNPs) were then used to place the gene in an interval covered by several cosmids. We next performed rescue experiments by injecting candidate cosmids and found that T05G5 rescued the Psa phenotype of *rmd-1(os21)*. A mutant named *tm1457* (isolated by the National Bioresource Project), which has a deletion affecting both T05G5.7 and T05G5.9, also showed the Psa phenotype and failed to complement *rmd-1(os21)* for both the Psa and maternal effect lethality phenotypes. The *T05G5.7* gene is located in an intron of the *T05G5.9* gene in the inverted orientation (Fig. 1).

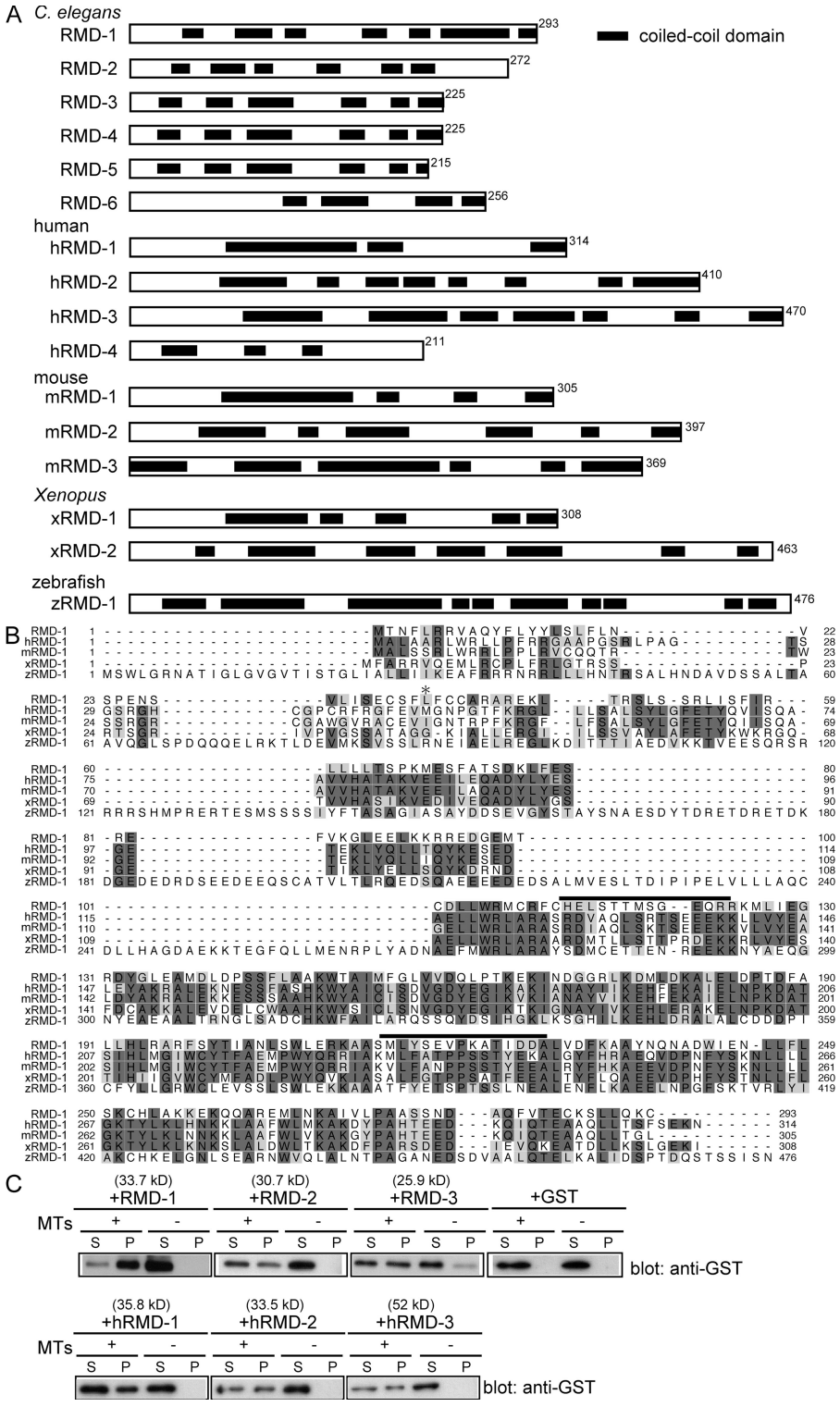

Figure 2. **Structure of the RMD proteins.** (A) Schematic presentation of RMD proteins. Black boxes indicate coiled-coil domains. The total length of each protein is indicated at the right. hRMD-1/cgi-90 was identified by comparative proteomics (Lai et al., 2000). hRMD-2/BLOCK18 was identified by a computational screen for secreted proteins (Clark et al., 2003). hRMD-3/cerebral protein-10 (GenBank/EMBL/DDBJ accession no. AB000782) and hRMD-4 (GenBank/EMBL/DDBJ accession no. AK095462) were identified from a study of human transcriptome and functional genomics (Ota et al., 2004). Mouse homologues mRMD-1 (GenBank/EMBL/DDBJ accession no. AK010421), mRMD-2 (GenBank/EMBL/DDBJ accession no. BC024059), and mRMD-3 (GenBank/EMBL/DDBJ accession no. BC055754; Strausberg et al., 2002); *Xenopus* homologues xRMD-1 (GenBank/EMBL/DDBJ accession no. BC054253) and xRMD-2 (GenBank/EMBL/DDBJ accession no. BC090235); and zebrafish homologue zRMD-1 (GenBank/EMBL/DDBJ accession no. BX936455) are presented. (B) Comparison of *C. elegans*, human, mouse, *Xenopus*, and zebrafish RMD-1 proteins. Identical amino acids among RMD-1 homologues are shaded with black. Similar amino acids are shaded with gray. The asterisk shows the position of the mutation in *rmd-1(os21)*. The regions marked with lines were used as antigens to prepare an anti–RMD-1 antibody. (C) Results of cosedimentation assay. Affinity-purified GST-fused RMD-1, -2, and -3, hRMD-1, -2, and -3, and GST as indicated at the top of the panels were incubated in the presence (+) or absence (−) of taxol-stabilized microtubules (MTs) and subjected to centrifugation. The pellets (P) and supernatants (S) were immunoblotted.

We investigated the DNA sequences in the predicted open reading frame of T05G5.7 and T05G5.9 in *rmd-1(os21)* and found a single missense mutation that changed leucine 36 to tryptophan in T05G5.7 (Fig. 2 B, asterisk). Furthermore, the Psa phenotype of *rmd-1(os21)* was rescued by a plasmid containing the entire *T05G5.7* gene and part of the *T05G5.9* gene but not by a plasmid containing a longer portion of T05G5.9 and only part of T05G5.7 (Fig. 1). In addition, an RNAi of T05G5.7 but not T05G5.9 causes embryonic lethality (Sonnichsen et al., 2005). Thus, we conclude that T05G5.7 is the *rmd-1* gene.

The *rmd-1* gene encodes a novel protein of 293 amino acids that contains multiple coiled-coil domains (Fig. 2 A). The coiled-coil domains were predicted by a program (http://www.ch.embnet.org/software/COILS_form.html). Database searches revealed five proteins of unknown function related to RMD-1 in *C. elegans* (Fig. 2 A). The amino acid identity between these

proteins and RMD-1 was 34% for RMD-2 (C27H6.4), 26% for RMD-3 (B0491.3), 24% for RMD-4 (F36H12.11), 20% for RMD-5 (T23B3.3), and 26% for RMD-6 (R13H9.1). BLAST searches for proteins similar to RMD-1 in other species revealed putative homologues in human, mouse, *Xenopus*, and zebrafish but not in *Drosophila* or yeast (Fig. 2, A and B). Therefore, we conclude that RMD-1 is a member of a novel protein family (hereafter called the RMD proteins) that is evolutionally conserved in other organisms.

We explored the expression pattern of RMD-1 in embryos using an antibody that was raised against it. The specificity of the antibody was examined by Western blotting using extracts of wild-type and *rmd-1(RNAi)* embryos (Fig. 3 B) and by immunostaining (Fig. 3 A). We found that RMD-1 colocalized with tubulin throughout the first cell cycle. Specifically, RMD-1 accumulated at the spindle poles and interzonal microtubule bundles during metaphase and anaphase but seemed not to localize to the central spindle at anaphase (Fig. 3 A, g and j) nor to the kinetochore and chromosomes. Therefore, we further analyzed the direct interactions of GST-fused RMD-1, -2, and -3 with microtubules using taxol-stabilized microtubules. When each RMD protein was incubated with taxol-stabilized microtubules and cosedimented by centrifugation, RMD-1, -2, and -3 but not control GST proteins were precipitated with the microtubules (Fig. 2 C). The human RMD (hRMD) proteins (hRMD-1, -2, and -3) localized to the spindle microtubules and spindle poles (Fig. 3 C and Fig. S1, available at http://www.jcb.org/cgi/content/full/jcb.200705108/DC1) during cell division as the RMD-1 protein did in *C. elegans*. In interphase, hRMD proteins were observed as dots in cytoplasm, and some of the dots colocalized to microtubule lattice (Fig. S1). Besides, hRMD-2 was observed as larger dots in the perinuclear region (Fig. S1). Cosedimentation assay showed that hRMD proteins interacted with microtubules (Fig. 2 C). These data indicate that RMD proteins represent an evolutionally conserved MAP family.

Chromosome segregation is abnormal in *rmd-1* embryos

To elucidate the functions of *rmd-1* during embryogenesis, we observed the phenotypes of *rmd-1* embryos. Because *rmd-1 (os21)* embryos showed only minor defects in early embryonic development compared with *rmd-1(RNAi)* embryos (see below for spindle orientation defects), we mostly analyzed *rmd-1 (RNAi)* embryos. We first found that *rmd-1(RNAi)* and *tm1457* but not *os21* embryos swelled, completely filling the space that normally lies between the egg shell and the embryo, suggesting that they are osmotically sensitive (Osm; Fig. S2 A, low salts; available at http://www.jcb.org/cgi/content/full/jcb.200705108/DC1). This phenotype was reported in a full-genome profile of *C. elegans* RNAi phenotypes (Sonnichsen et al., 2005). In addition to the Osm phenotype, *rmd-1(RNAi)* embryos showed defects in pronuclear meeting, pseudocleavage, cytokinesis, spindle orientation, and chromosome segregation (see Fig. S2 B and the next paragraph).

To analyze the functions of *rmd-1* in more detail, in all subsequent experiments, including controls, we used a high salt medium (see Materials and methods) in which the osmosensitivity of *rmd-1(RNAi)* embryos was rescued (Fig. S2 A, high salts; middle). Under this condition, the defects in pronuclear meeting, pseudocleavage, and cytokinesis were partially rescued, but those in spindle orientation, extrusion of polar bodies, and chromosome segregation (see the next paragraph) were not (Fig. S2 B), indicating that the latter defects are unlikely to be caused by the osmosensitivity. Nonetheless, it remained possible that these abnormalities in *rmd-1* embryos were caused by an egg shell defect that made the embryos sensitive to mechanical pressure from the coverslip. However, the mechanical causes for the abnormal spindle orientation, extrusion of polar body, and chromosome segregation are unlikely because these defects were not rescued by leaving a space between the embryos and coverslip to prevent pressure (Fig. S2 B, high salts with a space; and Fig. S3 C, available at http://www.jcb.org/cgi/content/full/jcb.200705108/DC1).

We further analyzed chromosome segregation using GFP-histone during mitosis and found that it was abnormal in the *rmd-1(RNAi)* embryos. During metaphase, the chromosomes did not align properly (100%; $n = 19$; Fig. 4 A, 1 min). At anaphase, the movement (elongation) of chromosomes along the spindle (Fig. 4 A, 4 min) was delayed compared with that in wild type (Fig. 4 A, 2 min 30 s). Chromosomes did not segregate but stretched laterally without separating into two masses until they were bisected by the cleavage furrow (Fig. 4 A, 4–9 min), indicating that chromosome segregation is defective in *rmd-1* embryos.

We next examined which abnormalities (meiosis, centromere resolution, sister chromatid separation, or microtubule attachments to kinetochores) caused the chromosome segregation defects in *rmd-1* embryos. First, we tested whether abnormal meiosis caused the chromosome segregation defect during mitosis. Although *rmd-1(RNAi)* embryos often showed defective extrusion of polar bodies, we did not observe defects in chromosome separation during meiosis in these embryos (Fig. S2 C). Consistent with this, immunostaining showed a normal meiotic spindle (Fig. S2 C, MTs). In addition, in *rmd-1* embryos with fewer (zero or one) polar bodies than wild-type embryos (two), we always observed multiple maternal pronuclei: two pronuclei in embryos with one polar body and three in those with no polar body (Fig. S2 D). Therefore, *rmd-1* embryos are specifically defective in the extrusion of polar bodies but not in nuclear divisions during meiosis.

To exclude the possibility that unextruded maternal DNA interfered with spindle formation in mitosis, we observed mitosis in *zen-4(RNAi)* embryos, in which the extrusion of polar bodies is defective (Raich et al., 1998), and did not find any lagging chromosomes (0%; $n = 5$; Fig. S2 D). These results indicate that unextruded maternal DNA does not interfere with the chromosome segregation in *rmd-1* embryos. Therefore, we conclude that mitotic chromosome segregation is specifically defective in *rmd-1(RNAi)* embryos.

Abnormal attachments of microtubules to kinetochores in *rmd-1* embryos

For proper chromosome segregation, sister centromeres must resolve from one another and take positions on the opposite

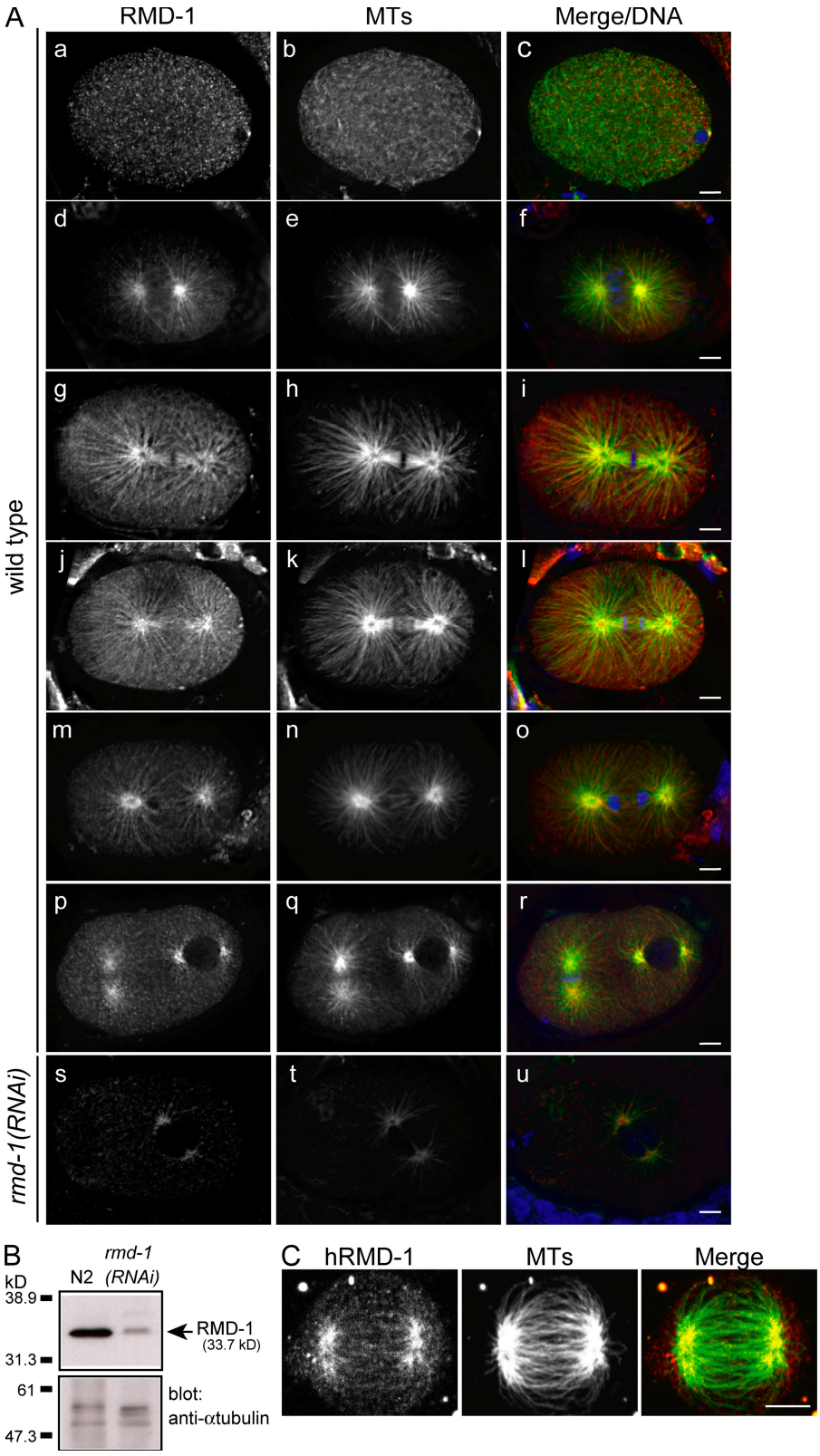

Figure 3. **RMD-1 and hRMD-1 localize to spindle microtubules and spindle poles during mitosis.** (A) Wild-type embryos were fixed and stained for RMD-1 and microtubules (MTs) during pronuclear migration (a–c), at the pronuclear meeting (d–f), metaphase (g–i), anaphase (j–l), telophase (m–o), and at the two-cell stage (p–r). Images of *rmd-1(RNAi)* embryos at the prometaphase stained for RMD-1 and microtubules (s–u). In the merged images, DNA is blue, RMD-1 is red, and microtubules are green. (B) Western blotting with anti–RMD-1. The lysates from wild-type embryos (N2) and *rmd-1(RNAi)* embryos were subjected to Western blotting using an anti–RMD-1 antibody. The numbers on the left show the positions of molecular weight markers. (C) HeLa cells expressing HA–hRMD-1 were fixed and stained for HA and microtubules during metaphase. In the merged image, hRMD-1 is red, and microtubules are green. Bars, 5 μm.

surfaces of chromosomes in early prophase, before microtubule capture (He and Brinkley, 1996). To investigate whether this process (centromere resolution) was defective in *rmd-1 (RNAi)* embryos, we observed the localization of a centromere protein, HCP-1/CENP-F, using HCP-1–GFP in live embryos (Fig. 5 A; Cheeseman et al., 2005). In *rmd-1(RNAi)* embryos, the HCP-1–GFP fluorescence appeared as two lines, as in wild-type embryos, during prometaphase (Fig. 5 A). Staining for the kinetochore protein KLP-7/MCAK also formed two lines along the chromosomes during prometaphase (Fig. 5 B).

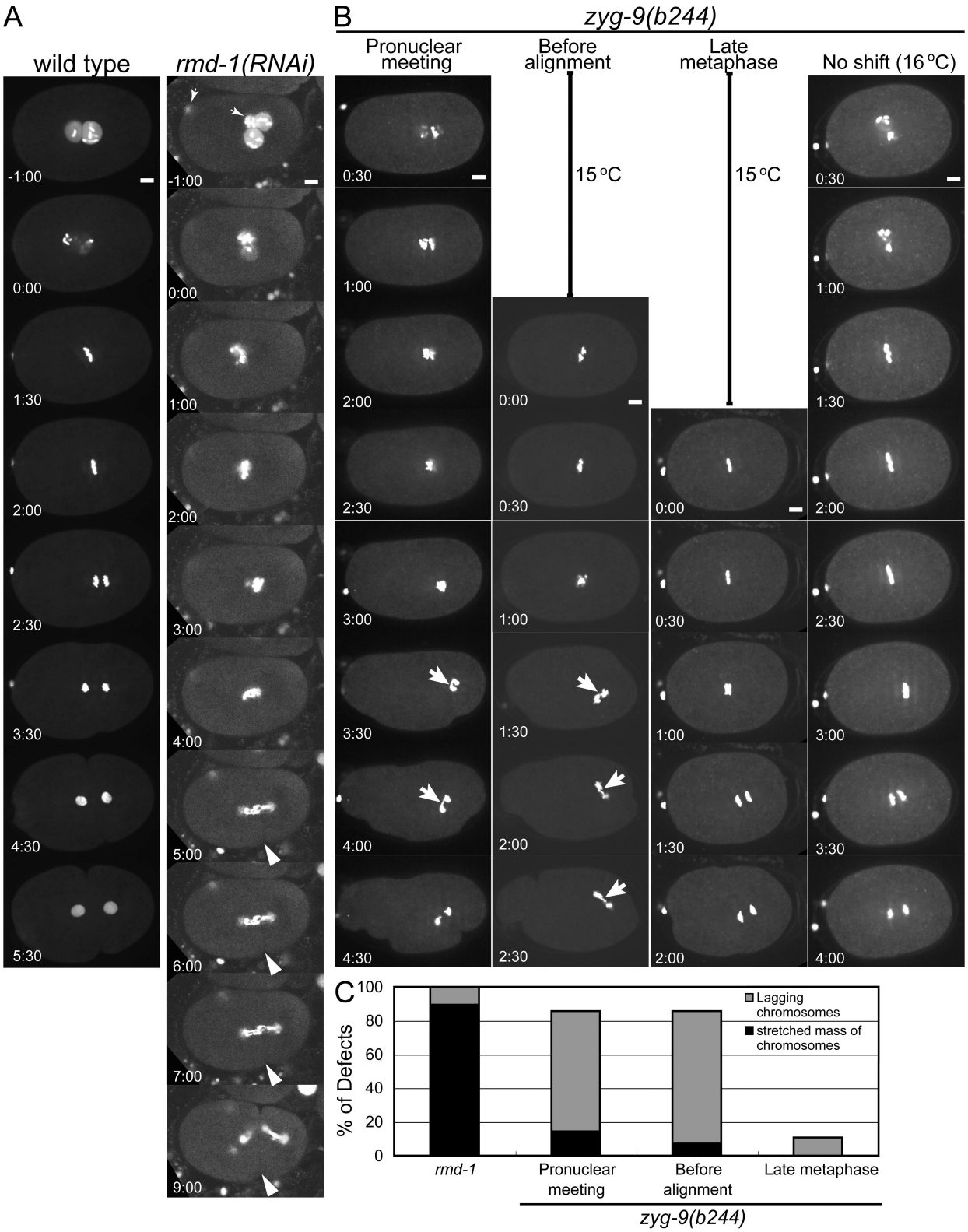

Figure 4. **Defects of *rmd-1(RNAi)* embryos in chromosome segregation.** (A) Time-lapse analyses of wild-type and *rmd-1(RNAi)* embryos expressing GFP-histone. In this *rmd-1(RNAi)* embryo, two maternal pronuclei (arrows), which failed to be extruded as polar bodies during meiosis, were detected, but they did not participate in the zygotic mitosis. In the *rmd-1(RNAi)* embryos, the chromosomes were not aligned on the metaphase plate in metaphase, and, in anaphase, the chromosomes were stretched along the axis of the spindle and failed to segregate. The position of the cleavage furrow in *rmd-1(RNAi)* embryos is indicated by arrowheads. The numbers on the left indicate the amount of time after NEBD. (B) Time-lapse images of *zyg-9(b244)* embryos expressing GFP-histone upshifted from 15 to 25°C at the stages indicated at the top of each column. Control embryos were observed at 16°C. The numbers on the left indicate the elapsed time after the start of observation (within 10 s after the upshift). The loss of ZYG-9 activity before metaphase caused lagging chromosomes, which are indicated by the arrows. (C) Percentages of embryos showing lagging chromosomes or a stretched mass of chromosomes in *rmd-1(RNAi)*

These results suggest that the centromere resolution is normal in *rmd-1* embryos.

Next, we analyzed sister chromatid separation by FISH analysis using a probe specific for the 5S ribosomal DNA (rDNA) repeats. In *rmd-1* embryos as in wild type, four individual FISH signals were always observed at anaphase ($n = 9$ for *rmd-1* and $n = 5$ for wild type; Fig. 5 C), indicating that sister chromatid cohesion resolves normally in *rmd-1(RNAi)* embryos.

The severe segregation defects in *rmd-1* embryos might be caused by abnormal attachments of microtubules to the kinetochores, such as merotelic attachments. To examine the microtubules' attachments to the kinetochores, we double stained the embryos for microtubules and the kinetochore protein KLP-7/MCAK. In wild-type embryos in prometaphase and anaphase, each chromosome interacted with kinetochore microtubules derived from only one of the spindle poles, and KLP-7/MCAK localized to the side of each chromosome that faced the pole (Fig. 5 D, wild type). If merotelic attachments were indeed present in the *rmd-1(RNAi)* embryos, we would expect to see chromosomes and kinetochores pulled from both spindle poles. As shown in Fig. 5 D, in *rmd-1(RNAi)* embryos at prometaphase, some chromosomes were located laterally (asterisks), and some microtubules (yellow arrows in prometaphase and dashed yellow lines in the magnified images) were crossed over chromosomes and kinetochores. In anaphase, the chromosomal DNA and KLP-7/MCAK (Fig. 5 D, yellow and light blue arrowheads) were located between two chromosome masses along abnormally extended microtubules (Fig. 5 D, yellow and light blue arrows) and appeared to be torn away from the masses of chromosomes. Furthermore, some microtubules (Fig. 5 D, anaphase; white arrows) extended toward the more distant chromosomes and kinetochores (Fig. 5 D, anaphase; white arrowheads). Similar defects in anaphase are observed in embryos with an *hcp-6* mutation, which causes merotelic attachments (Stear and Roth, 2002). These results suggest that the depletion of *rmd-1* causes merotelic attachments of microtubules to chromosomes (see the next section for more evidence).

RMD-1 interacts with aurora B kinase

It has been proposed that in other organisms, aurora B kinase functions to destabilize incorrectly attached microtubules (Maiato et al., 2004). Indeed, inactivation of aurora B induces multiple chromosome segregation defects in mammalian cells, including unsegregated chromosomes and lagging chromosomes (Kallio et al., 2002). Consistent with these findings, in *C. elegans*, embryos mutant for the aurora B homologue *air-2* show a laterally stretched mass of chromosomes, as we observed in *rmd-1* embryos (Kaitna et al., 2002). Therefore, it seemed possible that RMD-1 was involved in the AIR-2/aurora B–mediated correction mechanism. RMD-1 protein does not have any consensus sequences for aurora B phosphorylation, and we did not detect the phosphorylation of RMD-1 by aurora B in vitro (unpublished data). We then examined the interaction between RMD-1 and AIR-2 by pull-down assay. We found that FLAG-tagged AIR-2 protein produced in COS-7 cells coprecipitated with GST-fused RMD-1 but not with the GST protein alone (Fig. 6). Therefore, RMD-1 might function in chromosome segregation through an interaction with aurora B.

Abnormal kinetochore attachments cause a delay in spindle pole separation in *rmd-1* embryos

Because RMD-1 is a MAP, we also analyzed the spindle organization in live *rmd-1(RNAi)* embryos using GFP–β-tubulin (Fig. 7 A) and by immunostaining (Fig. 7 B). After the pronuclear meeting, the spindle poles moved to the center in wild-type embryos, and the posterior spindle pole then migrated in the posterior direction. During this process, long astral microtubules were detected in wild-type embryos (Figs. 4 B and 7 A, −30 min). In *rmd-1(RNAi)* embryos, the spindle failed to move completely to the center, and the astral microtubules were shorter and fewer (Fig. 7, A [−30 min] and B). During prometaphase and metaphase, in the *rmd-1(RNAi)* embryos, interzonal microtubules (including kinetochore microtubules) were observed, but the distances between the spindle poles were shorter, and the timing of the spindle pole separation was delayed compared with that in wild-type embryos (Fig. 7, A and C). At the two-cell stage, in wild-type embryos, the spindle in the AB cell was oriented transversely, and the one in the P1 cell was oriented in the anterior-posterior direction (Fig. S3). In *rmd-1 (RNAi)* embryos, the spindles in both the AB and P1 cells were oriented in an abnormal (nearly random) direction (Figs. S2 B and S3). Similar defects in spindle orientation were observed in *rmd-1(os21)* mutant embryos, in which the P1 cell showed incomplete spindle rotation, resulting in division along the transverse axis (10%; $n = 20$; Fig. S3 A). These phenotypes suggest that RMD-1 is required for correct spindle organization and positioning during mitosis.

In the *C. elegans* embryo, the majority of central spindle microtubules are attached to kinetochores, and these microtubule attachments restrain the spindle pole separation caused by astral pulling forces until sister chromatid cohesion is lost at anaphase onset (Grill and Hyman, 2005). As a result, the elimination of microtubule attachments to kinetochores by the depletion of *knl-1* causes premature pole separation (Fig. 7 C; Desai et al., 2003). Merotelic (but not syntelic) microtubule attachments would be predicted to restrain spindle pole separation even after anaphase onset. Indeed, the depletion of *rmd-1* caused a delay and slow spindle pole separation (Fig. 7 C). To test whether this slow pole separation was caused by merotelic microtubule attachment as opposed to weakened astral pulling forces, we asked whether the elimination of kinetochore–microtubule attachments

($n = 19$) and *zyg-9(b244)* embryos. Chromosomes that were uniformly stretched along the spindle were defined as a stretched mass of chromosomes. Chromosomes that were separated into two masses interconnected by chromatin bridges were scored as lagging chromosomes. The *zyg-9(b244)* embryos were upshifted from 15 to 25°C at the pronuclear meeting ($n = 7$), before chromosome alignment ($n = 14$), or during late metaphase ($n = 28$). Bars, 5 μm.

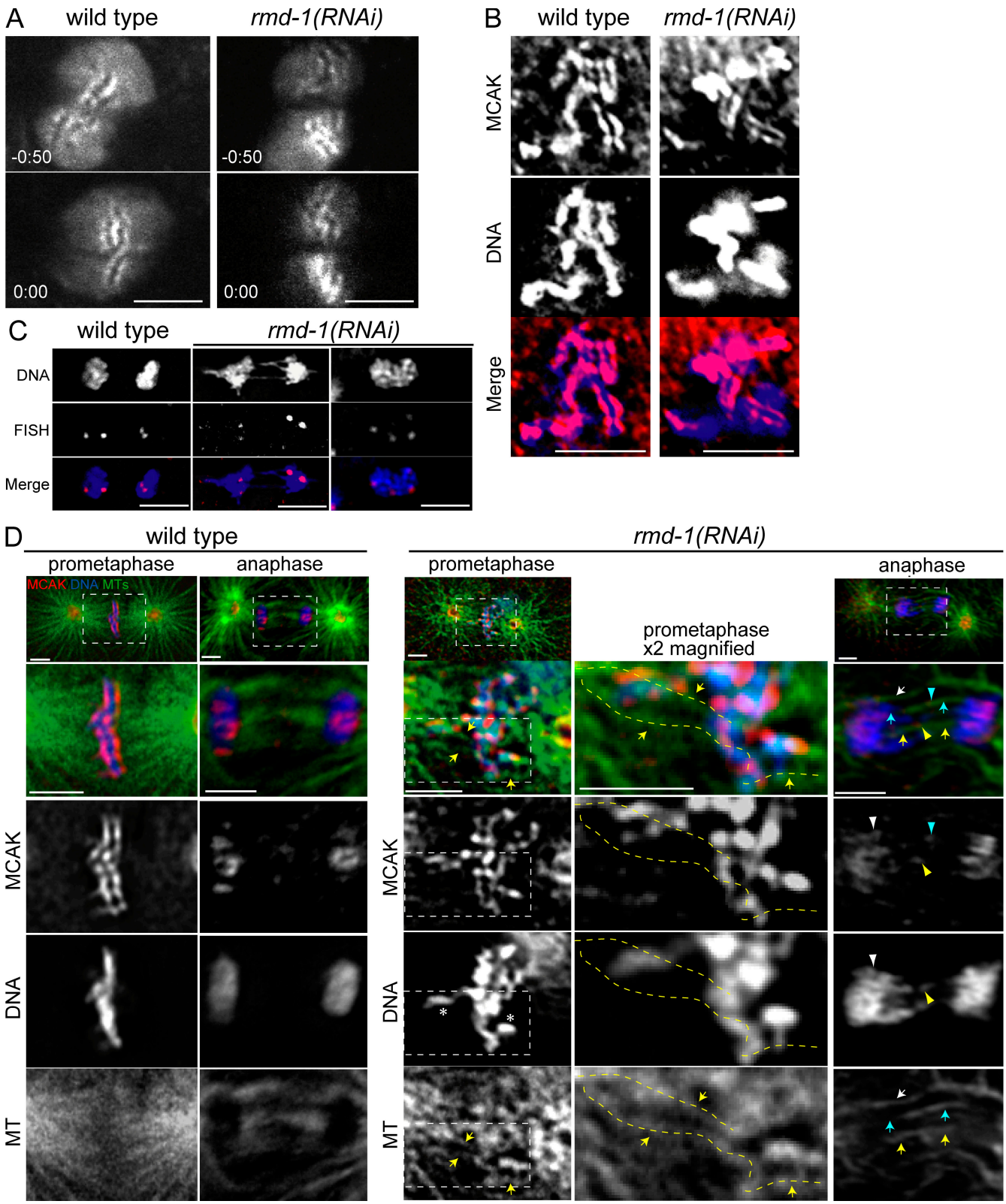

Figure 5. **Abnormal attachments of microtubules to kinetochores in *rmd-1(RNAi)* embryos.** (A) HCP-1–GFP was distributed in two lines in both wild-type and *rmd-1(RNAi)* embryos during prometaphase before NEBD. The number at the left in each panel is the elapsed time after NEBD. (B) In prometaphase before NEBD, KLP-7/MCAK was observed as two lines on the condensed chromosome in both wild-type and *rmd-1(RNAi)* embryos. In the merged images, MCAK is red, and DNA is blue. (C) Embryos in anaphase were fixed and processed for FISH using a 5S rDNA probe. In both wild-type and *rmd-1* embryos at anaphase, four discrete FISH signals were observed, indicating that sister chromatid cohesion was resolved. (D) Attachment of microtubules to kinetochores in wild-type and *rmd-1(RNAi)* embryos. Embryos were fixed and stained to label microtubules (MTs), MCAK, and DNA (with DAPI). In the merged images, microtubules are green, MCAK is red, DNA is blue, and microtubules that overlap with chromosomes are represented in light blue. In wild-type embryos at prometaphase after NEBD, chromosomes interacted with microtubules derived only from the closest spindle poles, but, in *rmd-1(RNAi)* embryos,

by the depletion of *knl-1* would suppress the pole separation defect in *rmd-1(RNAi)* embryos. As expected, in embryos depleted of both KNL-1 and RMD-1, the distance between the spindle poles and the delay in spindle pole separation became normal (Fig. 7 C). Together with the aforementioned results of immunostaining, our results suggest that the depletion of *rmd-1* causes the defects in spindle pole separation and chromosome segregation as a result of merotelic attachments of microtubules to chromosomes.

Abnormal chromosome segregation in *rmd-1* embryos is not caused by a defect in microtubule dynamics

The short astral microtubules in *rmd-1(RNAi)* embryos suggested that RMD-1 might regulate microtubule dynamics. Therefore, we examined the growth rate of the astral microtubules during mitosis by tracking the movement of the *C. elegans* EB1 homologue EBP-2–GFP, which reflects microtubule growth (Srayko et al., 2005). We recorded images at 200-ms intervals using a spinning disk confocal microscope and randomly selected EBP-2–GFP dots that remained in the focal plane for at least 3 s (Fig. 8 A). We found that the growth rate of microtubules during mitosis was reduced in *rmd-1(RNAi)* embryos compared with wild-type embryos at all stages of the cell cycle examined (Fig. 8 B and Videos 1 and 2, available at http://www.jcb.org/cgi/content/full/jcb.200705108/DC1). These results indicate that RMD-1 is required for the efficient growth of astral microtubules during mitosis.

In *C. elegans*, ZYG-9, a homologue of XMAP215, regulates the growth of microtubules (Matthews et al., 1998; Srayko et al., 2005). We examined the relationship between ZYG-9 and RMD-1 on the growth rate of microtubules using EBP-2–GFP. After nuclear envelope breakdown (NEBD), *zyg-9(RNAi)* embryos showed a much more severe defect in microtubule growth than that in *rmd-1(RNAi)* embryos (Fig. 8 B). In *rmd-1(RNAi)* + *zyg-9(RNAi)* embryos, the growth rate of astral microtubules was similar to that in *zyg-9(RNAi)* embryos (Fig. 8 B). However, because RMD-1's effect on microtubule growth was weak, it was difficult to determine the relationship between RMD-1 and ZYG-9 in this process.

The defects in the growth of astral microtubules raised the possibility that the abnormal kinetochore attachments in *rmd-1* embryos were also caused by this defect. If this was the case, *zyg-9* embryos, which show stronger defects in microtubule growth, should show chromosome segregation defects as in *rmd-1* embryos. To examine the roles of *zyg-9* specifically in chromosome segregation, we performed rapid temperature shift experiments using a temperature-sensitive mutant, *zyg-9(b244)*, which has severe defects in microtubule growth, similar to those seen in *zyg-9(RNAi)* embryos (Srayko et al., 2005). A temperature upshift of *zyg-9(b244)* embryos at the time of pronuclear meeting

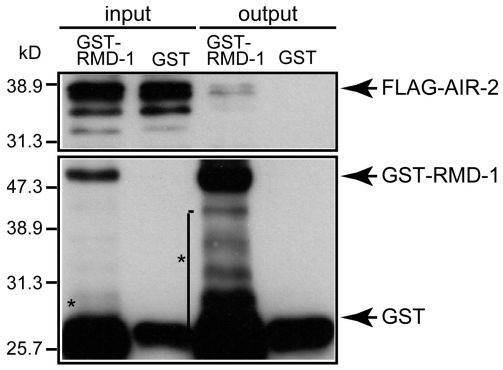

Figure 6. **RMD-1 interacts with aurora B kinase.** FLAG-tagged AIR-2 was coprecipitated with GST–RMD-1 but not with GST, indicating that RMD-1 interacts with AIR-2. Input shows 1/25 of cell lysate used in the experiments. Asterisks show degradation products.

immediately (within 2 min) induced short astral microtubules like those observed in the *zyg-9(RNAi)* embryos (Fig. S2 E), indicating that ZYG-9 activity responds quickly to the temperature shift. At the permissive temperature (16°C), *zyg-9(b244)* did not display any defects in chromosome segregation ($n = 5$; Fig. 4 B). An upshift in temperature at the time of pronuclear meeting or before alignment of all of the chromosomes on the metaphase plate induced lagging chromosomes, although the chromosomes were separated into two masses in most *zyg-9 (b244)* embryos (Fig. 4, B and C). In contrast, most embryos exposed to the higher temperature at late metaphase, when all of the chromosomes were aligned on the metaphase plate, did not have lagging chromosomes (Fig. 4, B and C). These results suggest that efficient microtubule outgrowth regulated by ZYG-9 is required for chromosome segregation. Therefore, the abnormal segregation in *rmd-1* embryos might also be caused by defects in microtubule outgrowth, at least in part. However, a mass of stretched chromosomes that was frequently observed in the *rmd-1* embryos was rare in *zyg-9(b244)* embryos (Fig. 4 C). Thus, the defects in the *rmd-1* embryos are unlikely to be explained simply by the slow growth of microtubules. Rather, our results suggest that RMD-1 has other important functions, possibly in the AIR-2/aurora B–mediated pathway, for the proper segregation of chromosomes.

Discussion

The role of RMD-1 in chromosome segregation

In this study, we have shown that the depletion of RMD-1 induces defects in mitotic chromosome segregation. Cytological analyses suggest that the resolution of centromere and sister chromatid cohesion occurs normally in *rmd-1* embryos. However, chromosomes in *rmd-1* embryos failed to congress or segregate

microtubules (yellow arrows) crossed over chromosomes and kinetochores (stained with anti-MCAK). Broken lines in the magnified image show microtubules that crossed over chromosomes and kinetochores. At anaphase, kinetochores and chromosomes (light blue and yellow arrowheads) appeared to be pulled toward the opposite pole along incorrectly attached microtubules (light blue and yellow arrows). In addition, microtubules (white arrows) that interacted with the more distant kinetochores and chromosomes (white arrowheads) were observed. The regions indicated by dashed boxes are magnified. The asterisks represent chromosomes that are laterally located. Bars (A–C), 5 μm; (D) 2.5 μm.

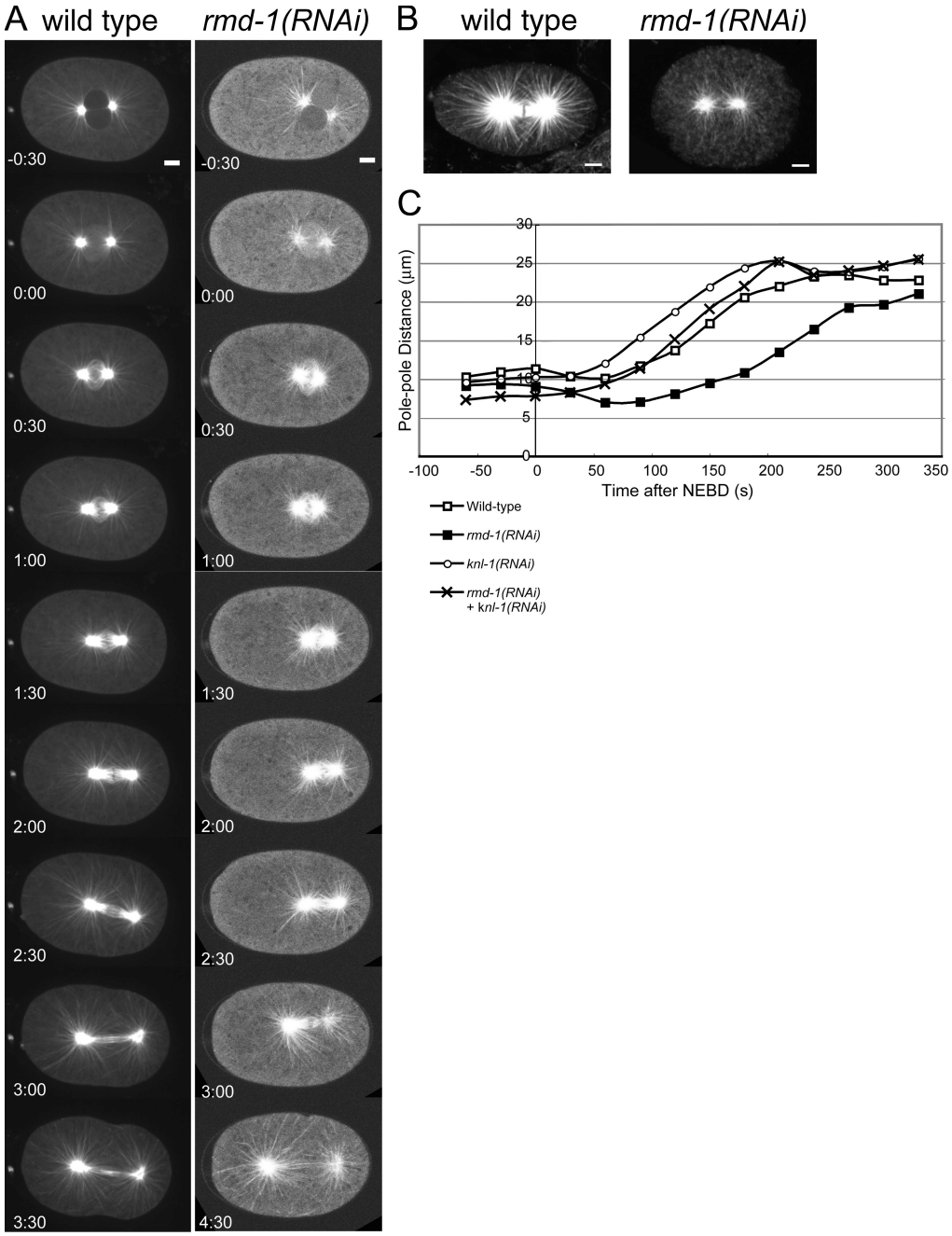

Figure 7. **Depletion of RMD-1 induces abnormal spindle organization.** (A) Time-lapse images of GFP–β-tubulin in wild-type and *rmd-1(RNAi)* embryos. Time after NEBD is indicated at the left. (B) Embryos were fixed and stained for tubulin using anti–α-tubulin. At the one-cell stage, long asters were observed in wild-type embryos. In contrast, short astral microtubules were observed in the *rmd-1(RNAi)* embryos. (C) The distance between the spindle poles was tracked in wild-type ($n = 9$; white squares), *rmd-1(RNAi)* ($n = 13$; black squares), *knl-1(RNAi)* ($n = 11$; white circles), and *knl-1(RNAi)* + *rmd-1(RNAi)* ($n = 8$; crosses) embryos. The plots show the mean distances between the spindle poles versus time after NEBD. Bars, 5 μm.

properly, resulting in unsegregated chromosomes. This phenomenon could be caused by the incorrect attachments of microtubules to kinetochores. Consistent with this interpretation, spindle pole separation during anaphase was delayed, and abnormal attachments were observed in *rmd-1* embryos. These results suggest that RMD-1 has important roles in the achievement of correct attachment between microtubules and kinetochores.

rmd-1 embryos showed a laterally stretched mass of chromosomes, suggesting that most chromosomes have incorrect attachments. This is surprising because, at least in mammalian cells, abnormal attachments are much less frequent, even in early mitosis. This chromosomal phenotype may be partly caused by the elongated kinetochore structure in *C. elegans*, which protrudes from the chromosome surface (Albertson and Thomson, 1982), creating more opportunity for microtubules to access incorrect kinetochores. In addition, the holocentric nature of *C. elegans* kinetochores may further increase the chances for abnormal attachments. In any case, such strong defects were rare in *zyg-9*

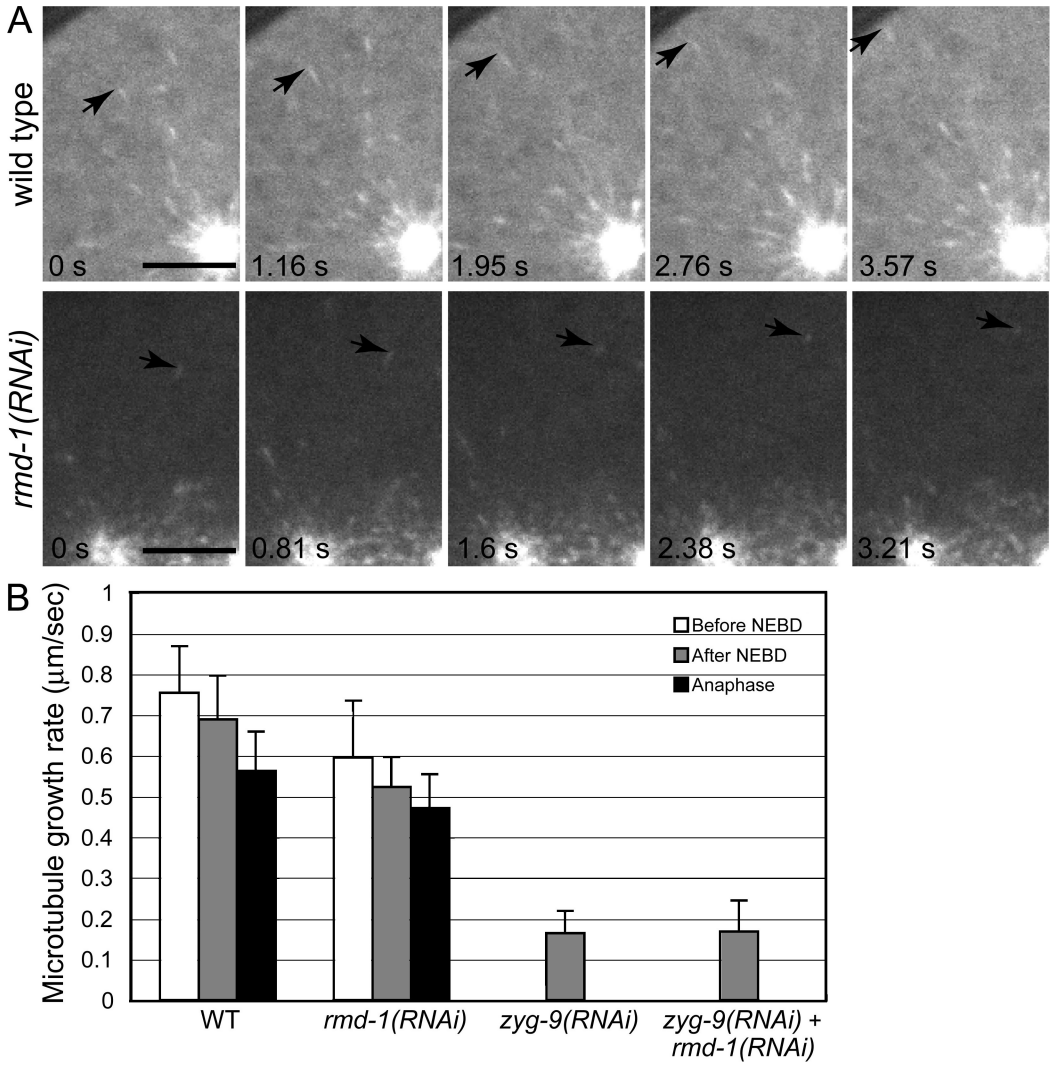

Figure 8. **RMD-1 is a novel MAP that regulates the dynamics of microtubules.** (A) Examples of tracking EBP-2–GFP dots obtained in live analyses. Each arrow indicates the position of a single dot of EBP-2–GFP whose movement was traced. (B) Microtubule growth rates calculated by speed of EBP-2 movement before NEBD (n = 48 for wild type and n = 48 for *rmd-1(RNAi)*), after NEBD (n = 70 for wild type, n = 65 for *rmd-1(RNAi)*, n = 21 for *zyg-9(RNAi)*, and n = 21 for *zyg-9 rmd-1(RNAi)*), and during anaphase (n = 30 for wild type and n = 40 for *rmd-1*). In *rmd-1(RNAi)* embryos, the growth rate of astral microtubules was significantly lower than in wild type ($P < 0.0001$ before NEBD, $P < 0.0001$ after NEBD, and $P = 0.00013$ during anaphase). In the *zyg-9(RNAi)* embryos, the additional RNAi against *rmd-1* had no significant additional effect on the microtubule growth rate after NEBD ($P = 0.82$). P-values were calculated by *t* test assuming unequal variances. Error bars represent SD. Bars, 5 μm.

embryos, and, thus, they cannot be explained solely by the slow growth of microtubules. Therefore, RMD-1 is likely to have more direct roles in the achievement of correct attachment.

Roles for aurora B in the correction of abnormal attachments have been proposed in mammalian cells (Shannon and Salmon, 2002; Lampson et al., 2004). In *C. elegans*, aurora B/*air-2* mutants show a stretched mass of chromosomes (Kaitna et al., 2002), suggesting that AIR-2 functions in the correct attachment between kinetochores and microtubules. The *rmd-1(RNAi)* embryos showed a stretched mass of chromosomes similar to that in the aurora B/*air-2* mutants. In addition, RMD-1 interacted with aurora B/AIR-2 in vitro. Therefore, RMD-1 could function to elicit proper chromosome segregation through the aurora B/AIR-2–mediated pathway. Further analyses will be necessary to elucidate how RMD-1 and AIR-2 cooperate to resolve incorrect attachments.

RMD-1 is a member of a novel but conserved MAP family

Our results show that RMD-1 is a member of a novel MAP family. We found homologues of RMD-1 in human, mouse, *Xenopus*, and zebrafish. Furthermore, hRMD proteins bound to and colocalized with microtubules, indicating that RMD proteins comprise an evolutionally conserved MAP family. The various microtubule-binding motifs of many MAPs have been identified (Chen et al., 1992; Cravchik et al., 1994; Leung et al., 1999; Schuyler and Pellman, 2001). However, we found no sequence homology of RMD proteins with other MAPs. Further analyses of RMD-1 may reveal novel microtubule-binding domains.

In addition to its regulation of chromosome segregation, our data indicate that RMD-1 functions in the growth of astral microtubules. Defects in this RMD-1 function might cause short astral microtubules and defective spindle orientation at the

two-cell stage in *rmd-1* embryos. How RMD-1 functions in microtubule growth is as yet unresolved. Although both RMD-1 and ZYG-9 regulate microtubule growth, we were not able to fully elucidate their relationship in this study. If RMD-1 is involved in ZYG-9–mediated microtubule growth, RMD-1 may modulate ZYG-9 activity to regulate microtubule dynamics. Further analyses of RMD-1's microtubule-binding properties and identification of its binding proteins will help elucidate the functions of RMD proteins in microtubule growth.

The regulatory factors aurora B kinase, INCENP, and Survivin, which function to ensure correct attachments in other eukaryotes, are conserved in *C. elegans* (Romano et al., 2003). Furthermore, RMD proteins are conserved and localize to spindles in mammalian cells. Therefore, the functions of RMD-1 may be evolutionally conserved and may be critical to achieve correct microtubule attachment during mitosis in other organisms as well.

Materials and methods

Strains

N2 bristol was used as the wild-type strain. The temperature-sensitive mutants *rmd-1(os21)* and *zyg-9(b244)* (Wood et al., 1980) were maintained as homozygotes at the permissive temperature of 15°C. The deletion mutant *tm1457* (a gift of S. Mitani, Tokyo Women's Medical University, Tokyo, Japan) was maintained as *tm1457*/hT2 at 22.5°C. Strain TH66 (a gift of M. Srayko, Max Plank Institute, Dresden, Germany) expressing EBP-2–GFP was maintained at 25°C (Srayko et al., 2005). The following integrated transgenes were used: *ruIs32* (*unc-119(+) pie-1- GFP-his-11*) for GFP-histone (Praitis et al., 2001), *ruIs48* (*unc-119(+) pie-1-GFP-tbb-1*) for GFP–β-tubulin (Strome et al., 2001), and *itIs3* (*unc-119(+) pie-1-hcp-1-GFP-TEV-STag*) for HCP-1–GFP (Cheeseman et al., 2005). The animals were maintained using standard procedures (Brenner, 1974).

Positional cloning and molecular characterization

rmd-1(os21) was mapped to *LGIII*. Three-point mapping was performed, which placed *rmd-1* between *ced-7* and *unc-69*. From heterozygotes of the genotype *sma-2 ced-7 unc-69/+ + rmd-1+*, non-Sma non-Ced Unc recombinants were obtained, and 13/19 segregated *rmd-1(os21)*. To map *rmd-1 (os21)* relative to SNPs, we mated CB4856 males and *rmd-1(os21) unc69* hermaphrodites, selected Unc non-Psa recombinants, plated them separately, identified self-progeny homozygotes, and checked for SNPs in these strains. *rmd-1(os21)* was mapped to the region just to the right of *T05G5*. Rescue experiments were performed using plasmids containing fragments amplified by PCR from T05G5 cosmids (pKO1, 27,122–35,387 bp; pKO2, 27,122–32,282 bp; pKO3, 27,122–31,384 bp; and pKO4, 29,620–31,940 bp) that were injected into *rmd-1(os21)* mutant larvae to test for rescue of the Psa phenotype. A cDNA clone, yk507f10, corresponding to T05G5.7 had the predicted coding sequence but did not include the first ATG. We identified the start codon by RT-PCR of RNAs from wild-type animals using primers against the trans-spliced SL1 leader and an internal region of T05G5.7. The PCR products were subcloned into pBST to generate pBSCr1.

RNA-mediated interference

To prepare double-stranded RNA, PCR with T7 and T3 primers was used to amplify cDNA fragments from yk507f10 (*rmd-1*), yk396b3 (*zyg-9*), yk444c6 (*knl-1*), and yk391b3 (*zen-4*; all yk cDNA clones are gifts of Y. Kohara, National Institute of Genetics, Mishima, Japan). RNA was synthesized using T3 and T7 polymerase (Promega). For all experiments, double-stranded RNAs were injected into L4 hermaphrodites. All animals injected with double- stranded RNA were incubated at 25°C for 20–28 h before observation.

Live imaging

To observe live embryos, the embryos were dissected from gravid hermaphrodites in high salt medium (0.5× embryonic growth medium [Edgar, 1995] supplemented with 1 M KCl). Under this condition, wild-type embryos did not show defects in early embryogenesis (Figs. 3–6, S3, and S4). For most observations, embryos were mounted on 5% agar pads under a coverslip, except for the experiments shown in Fig. S3 B (high salt with a space) and Fig. S4 C, in which embryos were mounted on poly-lysine–coated coverslips and inverted over 5% agar pads with a space between the embryos and a coverslip. Fluorescence images from GFP-histone, GFP–β-tubulin, HCP-1–GFP, and EBP-2–GFP were collected by a camera (Orca ER; Hamamatsu) mounted on a microscope using a 63× 1.4 NA plan-Apochromat objective (Carl Zeiss, Inc.) and disk head (Yokogawa) using IPLab software (BD Biosciences). Images were collected at intervals of 30 (GFP–β-tubulin and GFP-histone), 10 (HCP-1–GFP), or 0.2 s (GFP–EBP-2; 1 × 1 binning). EBP-2–GFP dots that remained in the focal plane for at least 3 s were randomly selected for tracking. Roughly five GFP dots were analyzed per centrosome in at least three embryos. The distance from each EBP-2–GFP dot to the centrosome was measured at each time interval. The growth rates of the microtubules were determined by calculating the mean velocity of the EBP-2 movements from the position at each time interval (Microsoft Excel).

For rapid temperature upshift experiments, embryos grown at 15°C were collected and mounted on slides with an agar pad at room temperature (~25°C) followed by quick observation to find the embryos before pronuclear migration (this entire procedure took 141 s on average and always <3 min). The slides were then placed on an aluminum block in the microscope room, which was kept at 15°C for at least 5 min until the events of interest occurred (timing of the temperature shifts is given in Fig. 5 B). The microscope room was kept at 25°C for the temperature shift experiments and at 16°C for experiments without a temperature shift.

Antibodies and immunofluorescence

An anti–RMD-1 rabbit antibody was generated against two C-terminal peptides of RMD-1 (Fig. 1 B) and was used at a 1:2,000 dilution. The following primary antibodies were also used: anti–α-tubulin antibody DMIA (1:500; Sigma-Aldrich), anti-GFP antibody (1:500; MBL International), anti-GFP 3E6 (1:500; Invitrogen), anti-GST antibody B-14 (1:10,000; Santa Cruz Biotechnology, Inc.), anti-HA antibody 3F6 (1:500; Roche), anti-FLAG M2 (1:1,000; Sigma-Aldrich), and anti–KLP-7/MCAK (1:1,000; a gift of K. Oegema and A. Desai, University of California, San Diego, La Jolla, CA; Oegema et al., 2001). The secondary antibodies were fluorescein-conjugated goat anti–mouse IgG, rhodamine red-X–conjugated goat anti–rabbit IgG, rhodamine-conjugated goat anti–mouse IgG, and Alexa-Fluor555-conjugated goat anti–rat IgG (Invitrogen) diluted 1:500.

Fixed embryos were incubated with primary antibody at room temperature for 2 h before being incubated with the appropriate secondary antibody for 2 h at room temperature. Three-color 3D image stacks were collected at 0.2-μm steps using a 100× 1.3 NA U-plan Apo objective (Olympus) and were computationally deconvolved by an imaging system (DeltaVision; Applied Precision).

FISH

The 5S rDNA probe was generated by PCR amplification of a single 1-kb repeated unit from the *C. elegans* genome using primers described previously (Dernburg et al., 1998). Probe DNA was enzymatically fragmented, 3′ end labeled using cy3-dUTP (GE Healthcare) and terminal deoxynucleotidyl transferase (Promega), and purified over a column (Sephadex G50). The labeled probe DNA was then precipitated from the eluent and resuspended in hybridization solution (BD Biosciences). FISH was performed as described previously (Kaitna et al., 2002) but replacing the hybridization buffer with BD Biosciences hybridization buffer.

Protein purification and cosedimentation assays

To generate a full-length cDNA clone (pBSr1) of *rmd-1*, a 628-bp XhoI fragment from yk507f10 was inserted into the XhoI site of pBSCr1. The fragment, including the entire *rmd-1* sequence, was amplified from pBSCr1. The PCR product was inserted into pGEX-4T-1 (GE Healthcare) to yield the pGEX-4T-1-RMD-1 plasmid. The fragments containing the full-length *rmd-2* and *rmd-3* genes from yk626b6 (*rmd-2*) and yk306d2 (*rmd-3*) were amplified by PCR. The resulting fragments from *rmd-2* and *rmd-3* were subcloned into pBST to generate pBSr2 and pBSr3, respectively. The full-length hRMD-1, -2, and -3 cDNAs were amplified from a human fetal brain cDNA library (Clontech Laboratories, Inc.). Each fragment was inserted into pGEX-4T-1 and pTB701-HA (Oishi et al., 2001). GST-fused proteins were expressed in *Escherichia coli*, affinity purified using glutathione–Sepharose 4B (GE Healthcare), and dialyzed against BRB80 (80 mM Pipes, 1 mM $MgCl_2$, and 1 mM EGTA, pH 6.8, with KOH; Hyman et al., 1992). For cosedimentation assays, taxol-stabilized microtubules were prepared as described previously (Desai and Walczak, 2001). In brief, 1 mg/ml tubulin purified

from bovine brain (MP Biomedicals) was precooled at 0°C for 5 min and spun in a TLA100 rotor (Beckman Coulter) at 90,000 rpm for 2 min at 2°C. Taxol was added to the supernatant stepwise to be equimolar with the tubulin. Taxol-stabilized microtubules were then mixed with each GST fusion protein, which had been precleared by centrifugation in a TLA100 rotor at 90,000 rpm for 15 min at 23°C and incubated with the taxol-stabilized microtubules at 37°C for 15 min. GST fusion proteins were cosedimented with microtubules in a single centrifugation step in a TLA100 rotor at 90,000 rpm for 5 min at 23°C. The pellets were washed with BRB80 containing 1 mM DTT and 10 μM taxol, and both pellets and supernatants were recovered and mixed with an equal volume of SDS-PAGE loading buffer.

Pull-down assay

Full-length *air-2* cDNA was amplified from expressed sequence tag yk665d12 by PCR and inserted into pTB701/FLAG (Oishi et al., 2001). COS-7 cells were transfected with pTB701/FLAG/AIR-2 by Lipofectamine (Invitrogen). COS-7 cells expressing FLAG-tagged AIR-2 were lysed in lysis buffer (0.5× PBS, 20 mM Hepes, pH 7.6, 1% NP-40, 50 mM β-glycerophosphate, 1 mM Na_3VO_4, and 1 mM DTT) supplemented with a cocktail of protease inhibitors (Nakalai Tesque). Extracts of cells expressing FLAG-tagged AIR-2 were incubated with GST-fused RMD-1 or GST and pulled down with glutathione–Sepharose 4B. Coprecipitated proteins were detected by Western blotting.

Cell culture and immunofluorescence

HeLa cells were cultured as described previously (Kitagawa et al., 1998; Oishi et al., 2001), seeded onto 13-mm coverslips in a 35-mm culture dish (10^5 cells), and transfected as described previously (Kitagawa et al., 1998). Fixation and immunostaining were performed as described previously (Oishi et al., 1999). Fluorescence images were acquired with a fluorescent microscope (IX71; Olympus) using a 100× 1.3 NA U-plan Apo objective (Olympus) and computational deconvolution.

Online supplemental material

Fig. S1 shows subcellular distribution of the human homologues of RMD-1. Fig. S2 shows that *rmd-1* embryos display various defects in microtubule-based processes. Fig. S3 shows abnormal spindle orientation in *rmd-1* embryos. Video 1 shows living wild-type embryos expressing EBP-2–GFP after NEBD. Video 2 shows a living *rmd-1(RNAi)* embryo expressing EBP-2–GFP after NEBD. Online supplemental material is available at http://www.jcb.org/cgi/content/full/jcb.200705108/DC1.

We thank Dr. Martin Srayko for the EBP-2–GFP strain, Dr. Karen Oegema and Dr. Arshad Desai for the antibody against KLP-7/MCAK and for helpful discussions, Dr. Yuji Kohara for the cDNA clones, Dr. Shohei Mitani for the deletion mutant (*tm1457*), Dr. Bruce Bowerman and Dr. Hiroyuki Ohkura for comments on the manuscript, and members of the Sawa laboratory for helpful discussions. Some other strains used here were provided by the *Caenorhabditis* Genetic Center.

This work was supported by a Special Postdoctoral Research Program from RIKEN (to K. Oishi) and by grants from the Japanese Ministry of Education, Culture, Sports, Science and Technology (to H. Sawa).

Submitted: 17 May 2007
Accepted: 16 November 2007

References

Albertson, D.G., and J.N. Thomson. 1982. The kinetochores of *Caenorhabditis elegans*. *Chromosoma*. 86:409–428.

Brenner, S. 1974. The genetics of *Caenorhabditis elegans*. *Genetics*. 77:71–94.

Cheeseman, I.M., I. MacLeod, J.R. Yates III, K. Oegema, and A. Desai. 2005. The CENP-F-like proteins HCP-1 and HCP-2 target CLASP to kinetochores to mediate chromosome segregation. *Curr. Biol.* 15:771–777.

Chen, J., Y. Kanai, N.J. Cowan, and N. Hirokawa. 1992. Projection domains of MAP2 and tau determine spacings between microtubules in dendrites and axons. *Nature*. 360:674–677.

Cimini, D., and F. Degrassi. 2005. Aneuploidy: a matter of bad connections. *Trends Cell Biol.* 15:442–451.

Cimini, D., B. Moree, J.C. Canman, and E.D. Salmon. 2003. Merotelic kinetochore orientation occurs frequently during early mitosis in mammalian tissue cells and error correction is achieved by two different mechanisms. *J. Cell Sci.* 116:4213–4225.

Clark, H.F., A.L. Gurney, E. Abaya, K. Baker, D. Baldwin, J. Brush, J. Chen, B. Chow, C. Chui, C. Crowley, et al. 2003. The secreted protein discovery initiative (SPDI), a large-scale effort to identify novel human secreted and transmembrane proteins: a bioinformatics assessment. *Genome Res.* 13:2265–2270.

Cravchik, A., D. Reddy, and A. Matus. 1994. Identification of a novel microtubule-binding domain in microtubule-associated protein 1A (MAP1A). *J. Cell Sci.* 107:661–672.

Dernburg, A.F., K. McDonald, G. Moulder, R. Barstead, M. Dresser, and A.M. Villeneuve. 1998. Meiotic recombination in *C. elegans* initiates by a conserved mechanism and is dispensable for homologous chromosome synapsis. *Cell*. 94:387–398.

Desai, A., and C.E. Walczak. 2001. Assays for microtubule-destabilizing kinesins. *Methods Mol. Biol.* 164:109–121.

Desai, A., S. Rybina, T. Muller-Reichert, A. Shevchenko, A. Hyman, and K. Oegema. 2003. KNL-1 directs assembly of the microtubule-binding interface of the kinetochore in *C. elegans*. *Genes Dev.* 17:2421–2435.

Edgar, L.G. 1995. Blastomere culture and analysis. *Methods Cell Biol.* 48:303–321.

Grill, S.W., and A.A. Hyman. 2005. Spindle positioning by cortical pulling forces. *Dev. Cell*. 8:461–465.

He, D., and B.R. Brinkley. 1996. Structure and dynamic organization of centromeres/prekinetochores in the nucleus of mammalian cells. *J. Cell Sci.* 109:2693–2704.

Hyman, A.A., S. Salser, D.N. Drechsel, N. Unwin, and T.J. Mitchison. 1992. Role of GTP hydrolysis in microtubule dynamics: information from a slowly hydrolyzable analogue, GMPCPP. *Mol. Biol. Cell*. 3:1155–1167.

Inoue, Y.H., M. do Carmo Avides, M. Shiraki, P. Deak, M. Yamaguchi, Y. Nishimoto, A. Matsukage, and D.M. Glover. 2000. Orbit, a novel microtubule-associated protein essential for mitosis in *Drosophila melanogaster*. *J. Cell Biol.* 149:153–166.

Kaitna, S., P. Pasierbek, M. Jantsch, J. Loidl, and M. Glotzer. 2002. The aurora B kinase AIR-2 regulates kinetochores during mitosis and is required for separation of homologous chromosomes during meiosis. *Curr. Biol.* 12:798–812.

Kallio, M.J., M.L. McCleland, P.T. Stukenberg, and G.J. Gorbsky. 2002. Inhibition of aurora B kinase blocks chromosome segregation, overrides the spindle checkpoint, and perturbs microtubule dynamics in mitosis. *Curr. Biol.* 12:900–905.

Kitagawa, M., H. Mukai, M. Takahashi, and Y. Ono. 1998. The role of PKN in the regulation of alphaB-crystallin expression via heat shock transcription factor 1. *Biochem. Biophys. Res. Commun.* 252:561–565.

Kline-Smith, S.L., A. Khodjakov, P. Hergert, and C.E. Walczak. 2004. Depletion of centromeric MCAK leads to chromosome congression and segregation defects due to improper kinetochore attachments. *Mol. Biol. Cell*. 15:1146–1159.

Lai, C.H., C.Y. Chou, L.Y. Ch'ang, C.S. Liu, and W. Lin. 2000. Identification of novel human genes evolutionarily conserved in *Caenorhabditis elegans* by comparative proteomics. *Genome Res.* 10:703–713.

Lampson, M.A., K. Renduchitala, A. Khodjakov, and T.M. Kapoor. 2004. Correcting improper chromosome-spindle attachments during cell division. *Nat. Cell Biol.* 6:232–237.

Lemos, C.L., P. Sampaio, H. Maiato, M. Costa, L.V. Omel'yanchuk, V. Liberal, and C.E. Sunkel. 2000. Mast, a conserved microtubule-associated protein required for bipolar mitotic spindle organization. *EMBO J.* 19:3668–3682.

Leung, C.L., D. Sun, M. Zheng, D.R. Knowles, and R.K. Liem. 1999. Microtubule actin cross-linking factor (MACF): a hybrid of dystonin and dystrophin that can interact with the actin and microtubule cytoskeletons. *J. Cell Biol.* 147:1275–1286.

Lew, D.J., and D.J. Burke. 2003. The spindle assembly and spindle position checkpoints. *Annu. Rev. Genet.* 37:251–282.

Maiato, H., P. Sampaio, C.L. Lemos, J. Findlay, M. Carmena, W.C. Earnshaw, and C.E. Sunkel. 2002. MAST/Orbit has a role in microtubule-kinetochore attachment and is essential for chromosome alignment and maintenance of spindle bipolarity. *J. Cell Biol.* 157:749–760.

Maiato, H., P. Sampaio, and C.E. Sunkel. 2004. Microtubule-associated proteins and their essential roles during mitosis. *Int. Rev. Cytol.* 241:53–153.

Matthews, L.R., P. Carter, D. Thierry-Mieg, and K. Kemphues. 1998. ZYG-9, a *Caenorhabditis elegans* protein required for microtubule organization and function, is a component of meiotic and mitotic spindle poles. *J. Cell Biol.* 141:1159–1168.

Mitchison, T., and M. Kirschner. 1984. Dynamic instability of microtubule growth. *Nature*. 312:237–242.

Musacchio, A., and K.G. Hardwick. 2002. The spindle checkpoint: structural insights into dynamic signalling. *Nat. Rev. Mol. Cell Biol.* 3:731–741.

Oegema, K., A. Desai, S. Rybina, M. Kirkham, and A.A. Hyman. 2001. Functional analysis of kinetochore assembly in *Caenorhabditis elegans*. *J. Cell Biol.* 153:1209–1226.

Ohi, R., M.L. Coughlin, W.S. Lane, and T.J. Mitchison. 2003. An inner centromere protein that stimulates the microtubule depolymerizing activity of a KinI kinesin. *Dev. Cell*. 5:309–321.

Ohkura, H., M.A. Garcia, and T. Toda. 2001. Dis1/TOG universal microtubule adaptors - one MAP for all? *J. Cell Sci.* 114:3805–3812.

Oishi, K., H. Mukai, H. Shibata, M. Takahashi, and Y. Ona. 1999. Identification and characterization of PKNbeta, a novel isoform of protein kinase PKN: expression and arachidonic acid dependency are different from those of PKNalpha. *Biochem. Biophys. Res. Commun.* 261:808–814.

Oishi, K., M. Takahashi, H. Mukai, Y. Banno, S. Nakashima, Y. Kanaho, Y. Nozawa, and Y. Ono. 2001. PKN regulates phospholipase D1 through direct interaction. *J. Biol. Chem.* 276:18096–18101.

Ota, T., Y. Suzuki, T. Nishikawa, T. Otsuki, T. Sugiyama, R. Irie, A. Wakamatsu, K. Hayashi, H. Sato, K. Nagai, et al. 2004. Complete sequencing and characterization of 21,243 full-length human cDNAs. *Nat. Genet.* 36:40–45.

Pinsky, B.A., and S. Biggins. 2005. The spindle checkpoint: tension versus attachment. *Trends Cell Biol.* 15:486–493.

Praitis, V., E. Casey, D. Collar, and J. Austin. 2001. Creation of low-copy integrated transgenic lines in *Caenorhabditis elegans*. *Genetics*. 157:1217–1226.

Raich, W.B., A.N. Moran, J.H. Rothman, and J. Hardin. 1998. Cytokinesis and midzone microtubule organization in *Caenorhabditis elegans* require the kinesin-like protein ZEN-4. *Mol. Biol. Cell*. 9:2037–2049.

Romano, A., A. Guse, I. Krascenicova, H. Schnabel, R. Schnabel, and M. Glotzer. 2003. CSC-1: a subunit of the Aurora B kinase complex that binds to the survivin-like protein BIR-1 and the incenp-like protein ICP-1. *J. Cell Biol.* 161:229–236.

Sawa, H., H. Kouike, and H. Okano. 2000. Components of the SWI/SNF complex are required for asymmetric cell division in *C. elegans*. *Mol. Cell*. 6:617–624.

Schuyler, S.C., and D. Pellman. 2001. Microtubule "plus-end-tracking proteins": the end is just the beginning. *Cell*. 105:421–424.

Shannon, K.B., and E.D. Salmon. 2002. Chromosome dynamics: new light on Aurora B kinase function. *Curr. Biol.* 12:R458–R460.

Sonnichsen, B., L.B. Koski, A. Walsh, P. Marschall, B. Neumann, M. Brehm, A.M. Alleaume, J. Artelt, P. Bettencourt, E. Cassin, et al. 2005. Full-genome RNAi profiling of early embryogenesis in *Caenorhabditis elegans*. *Nature*. 434:462–469.

Srayko, M., A. Kaya, J. Stamford, and A.A. Hyman. 2005. Identification and characterization of factors required for microtubule growth and nucleation in the early *C. elegans* embryo. *Dev. Cell*. 9:223–236.

Stear, J.H., and M.B. Roth. 2002. Characterization of HCP-6, a *C. elegans* protein required to prevent chromosome twisting and merotelic attachment. *Genes Dev.* 16:1498–1508.

Strausberg, R.L., E.A. Feingold, L.H. Grouse, J.G. Derge, R.D. Klausner, F.S. Collins, L. Wagner, C.M. Shenmen, G.D. Schuler, and S.F. Altschul. 2002. Generation and initial analysis of more than 15,000 full-length human and mouse cDNA sequences. *Proc. Natl. Acad. Sci. USA*. 99:16899–16903.

Strome, S., J. Powers, M. Dunn, K. Reese, C.J. Malone, J. White, G. Seydoux, and W. Saxton. 2001. Spindle dynamics and the role of γ-tubulin in early *Caenorhabditis elegans* embryos. *Mol. Biol. Cell*. 12:1751–1764.

Tanaka, T.U., N. Rachidi, C. Janke, G. Pereira, M. Galova, E. Schiebel, M.J. Stark, and K. Nasmyth. 2002. Evidence that the Ipl1-Sli15 (Aurora kinase-INCENP) complex promotes chromosome bi-orientation by altering kinetochore-spindle pole connections. *Cell*. 108:317–329.

Wood, W.B., R. Hecht, S. Carr, R. Vanderslice, N. Wolf, and D. Hirsh. 1980. Parental effects and phenotypic characterization of mutations that affect early development in *Caenorhabditis elegans*. *Dev. Biol.* 74:446–469.